



**HAL**  
open science

## Field Investigation of Serpentinite With Induced Polarization and the K-Means Clustering Technique

André Revil, A Ghorbani, J Jacquet, S Barde-cabusson, H Chen, J Richard, P Vaudelet, G Ménard, J J Delannoy

► **To cite this version:**

André Revil, A Ghorbani, J Jacquet, S Barde-cabusson, H Chen, et al.. Field Investigation of Serpentinite With Induced Polarization and the K-Means Clustering Technique. *Geophysical Research Letters*, 2024, 51, 10.1029/2024gl108920 . hal-04729140

**HAL Id: hal-04729140**

**<https://hal.science/hal-04729140v1>**

Submitted on 9 Oct 2024

**HAL** is a multi-disciplinary open access archive for the deposit and dissemination of scientific research documents, whether they are published or not. The documents may come from teaching and research institutions in France or abroad, or from public or private research centers.

L'archive ouverte pluridisciplinaire **HAL**, est destinée au dépôt et à la diffusion de documents scientifiques de niveau recherche, publiés ou non, émanant des établissements d'enseignement et de recherche français ou étrangers, des laboratoires publics ou privés.



Distributed under a Creative Commons Attribution - NonCommercial - NoDerivatives 4.0 International License




# Geophysical Research Letters®



## RESEARCH LETTER

10.1029/2024GL108920

## Field Investigation of Serpentinite With Induced Polarization and the K-Means Clustering Technique

A. Revil<sup>1</sup> , A. Ghorbani<sup>2</sup>, J. Jacquet<sup>1</sup>, S. Barde-Cabusson<sup>3</sup>, H. Chen<sup>4</sup>, J. Richard<sup>2</sup> , P. Vaudelet<sup>2</sup> , G. Ménard<sup>1</sup>, and J. J. Delannoy<sup>1</sup>

<sup>1</sup>Université Savoie Mont-Blanc, CNRS, UMR CNRS 5204, EDYTEM, Le Bourget-du-Lac, France, <sup>2</sup>Naga Geophysics, Technolac, Le Bourget du Lac, France, <sup>3</sup>Geosciences Barcelona (GEO3BCN), CSIC, Barcelona, Spain, <sup>4</sup>ETH Zurich, Zürich, Switzerland

### Key Points:

- The chargeability of serpentinite is high because of the presence of magnetite
- Time-domain induced polarization tomography images serpentinite in the field
- Laboratory experiments and a clustering technique help to discriminate serpentinite

### Correspondence to:

A. Revil,  
[andre.revil@univ-smb.fr](mailto:andre.revil@univ-smb.fr)

### Citation:

Revil, A., Ghorbani, A., Jacquet, J., Barde-Cabusson, S., Chen, H., Richard, J., et al. (2024). Field investigation of serpentinite with induced polarization and the K-means clustering technique. *Geophysical Research Letters*, 51, e2024GL108920. <https://doi.org/10.1029/2024GL108920>

Received 20 FEB 2024  
Accepted 21 AUG 2024

**Abstract** We performed a field induced polarization survey at Rocher du Chateau in the French Alps. This site is characterized by the presence of ophiolites with an outcrop of serpentinites. Serpentinite is characterized by high resistivity (~0.5–10 kΩ m) and high chargeability (~20–400 mV V<sup>-1</sup>) values. We collected two serpentinite core samples for spectral induced polarization measurements conducted in the frequency range 10 mHz–45 kHz, validating the field results. The high chargeability of serpentinite is associated with the production of magnetite during the fluid-rock alteration, as indicated by the high magnetic susceptibility of the core samples (0.0340 SI). Using the laboratory measurements and the K-means clustering technique, we successfully imaged the serpentinite facies and we were able to distinguish blocks of serpentinites embedded in the sedimentary cover. This approach could possibly be used for the seafloor exploration using induced polarization.

**Plain Language Summary** Induced polarization is a non-invasive geophysical method known to be sensitive to the presence of semi-conductors. Serpentinite is formed through the alteration of peridotites, resulting in the formation of magnetite, which, in addition to its magnetic properties, is responsible for a strong chargeability. The presence of an ophiolite in the French Alps provides an exceptional opportunity to study on-shore the induced polarization response of peridotites, and especially serpentinite. The results obtained in this paper may prove to be useful for the exploration of the oceanic seafloors by documenting the properties of such materials.

## 1. Introduction

Outcrops of ultramafic rocks along mid-ocean ridges present distinct degrees of serpentinization associated with hydrothermal alteration processes (Toft et al., 1990). Through hydrothermal alteration, primary ferromagnesian minerals (e.g., olivine and pyroxenes) are transformed to secondary minerals including brucite, serpentine, and magnetite (Toft et al., 1990). Degree of hydrothermal alteration is key to understanding mechanical and transport properties of oceanic lithosphere (Carlson & Miller, 1997; Collettini et al., 2009; Vinciguerra & Bernabé, 2009). The serpentinization of peridotites affects their geophysical properties including their mass density (affecting in turn the gravity field), their magnetic properties, and their electrical properties including their chargeability (Chen et al., 2021, and references therein). Chargeability reflects the ability of a rock to store reversibly electrical charge under the influence of an external electrical field.

Induced polarization is a geophysical technique measuring both the electrical conductivity and chargeability of rocks and sediments (e.g., Revil, 2013; Schlumberger, 1920). Chen et al. (2021) were the first to describe induced polarization properties of peridotites and the effect of serpentinization because of the formation of magnetite. To our knowledge, this is the only work investigating the induced polarization properties of serpentinized peridotites in the laboratory and we are not aware of any field investigations of the induced polarization properties of serpentinites.

There are actually very few opportunities to study serpentinites on-shore. So we have to take advantage of the existence of ophiolites in the studied valley to see how induced polarization tomography can be applied to the characterization of such formations. Ophiolites are remnants of uplifted oceanic crust and upper mantle composed of gabbro and peridotite (Dilek, 2003; Hacker, 1990). An exposed example is in the French Alps at Rocher du Chateau which we chose as our test site (Figure 1). The geophysical survey consists of two profiles in both

© 2024. The Author(s).

This is an open access article under the terms of the [Creative Commons Attribution-NonCommercial-NoDerivs License](https://creativecommons.org/licenses/by/4.0/), which permits use and distribution in any medium, provided the original work is properly cited, the use is non-commercial and no modifications or adaptations are made.

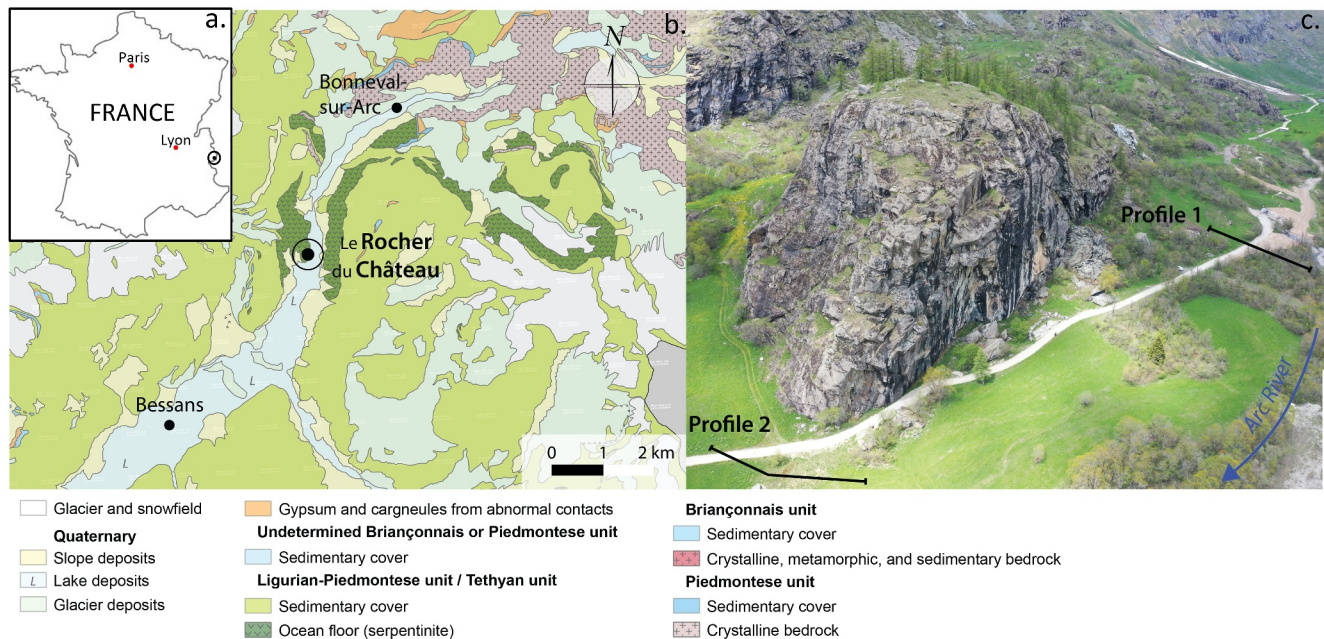


**Figure 1.** Position of the test site of Rocher-du-Chateau in France, geology and position of the profile. (a) Position of the test site on the map of France. (b) Rocher-du-Chateau in its geological context. (c) Picture of the Rocher-du-Chateau, near Bonneval-sur-Arc, showing also serpentinite blocks at the base of the cliff. The two profiles reported in this paper are denoted as Profile 1 and Profile 2.

resistivity (the inverse of conductivity) and chargeability tomography to obtain the characteristics of serpentinite in the field. The first profile was chosen in an area where serpentinites are outcropping. The second profile was chosen nearby, in an area where both large boulders of serpentinites and alluvium rich in serpentinite blocks are known to be present in the sedimentary cover (some boulders can be observed at the feet of the cliff shown in Figure 1b).

## 2. Site Description

Both geophysical profiles were acquired in the summer 2022 at Rocher du Chateau, Bessans, (Maurienne) France (Figures 1a and 1b). At a regional scale, this area belongs to the interior of the Western Alps where lustrous schists are covering an ophiolitic substratum related to the Eocene closure of the Tethys Ocean, 50 Ma ago (Chopin, 1979; Decrausaz et al., 2021; Lagabrielle, 1994). In the studied area, green rocks associated with ophiolites correspond to the lower section of the lustrous schist formation (Raguin, 1929; Robert, 1979), which form a vast reclining fold at the kilometer scale (Deville, 1987). In the vicinity of the studied site, the valley floor and the lower-half valley slopes are composed of serpentinites (magnetite-rich peridotites altered through hydrothermal leaching, see Deville, 1987; Fudral, 1998).

At the beginning of Profile 1 (Figure 1b), a nearly vertical wall of serpentinite dominates the landscape, while quaternary alluvial terraces shape the valley floor. The lower terrace (+2 m from the river level) corresponds to recent river deposits (Holocene). A higher terrace (+5 to 8 m from the river level) is possibly associated with an early holocene local lake episode (potential peri-deltaic deposit). Part of a glacial retreat moraine could have been partially preserved, embedded into that fine-sandy and silty formation. During the last glacial episode (MIS2, alpine Würm), the Maurienne valley was covered by the Arc glacier, until the younger Dryas (c. 12,900 to 11,700 years BP, see Nicoud et al. (2009)). Part of the sedimentary cover, including the potential moraine mentioned above, results from the last deglaciation events. Finally, massive boulders (side length of several meters) of serpentinites collapsed from the rock wall (Figure 1b). They can be observed on or partially embedded in the sedimentary cover (terraces).

## 3. Field and Laboratory Measurements

Two profiles (Figures 2 and 3) were performed using an ABEM SAS4000 impedance meter and a cable with a separation of 1 m between the take-outs (positions Figure 1b, each profile is ~63 m long). Sixty-four stainless

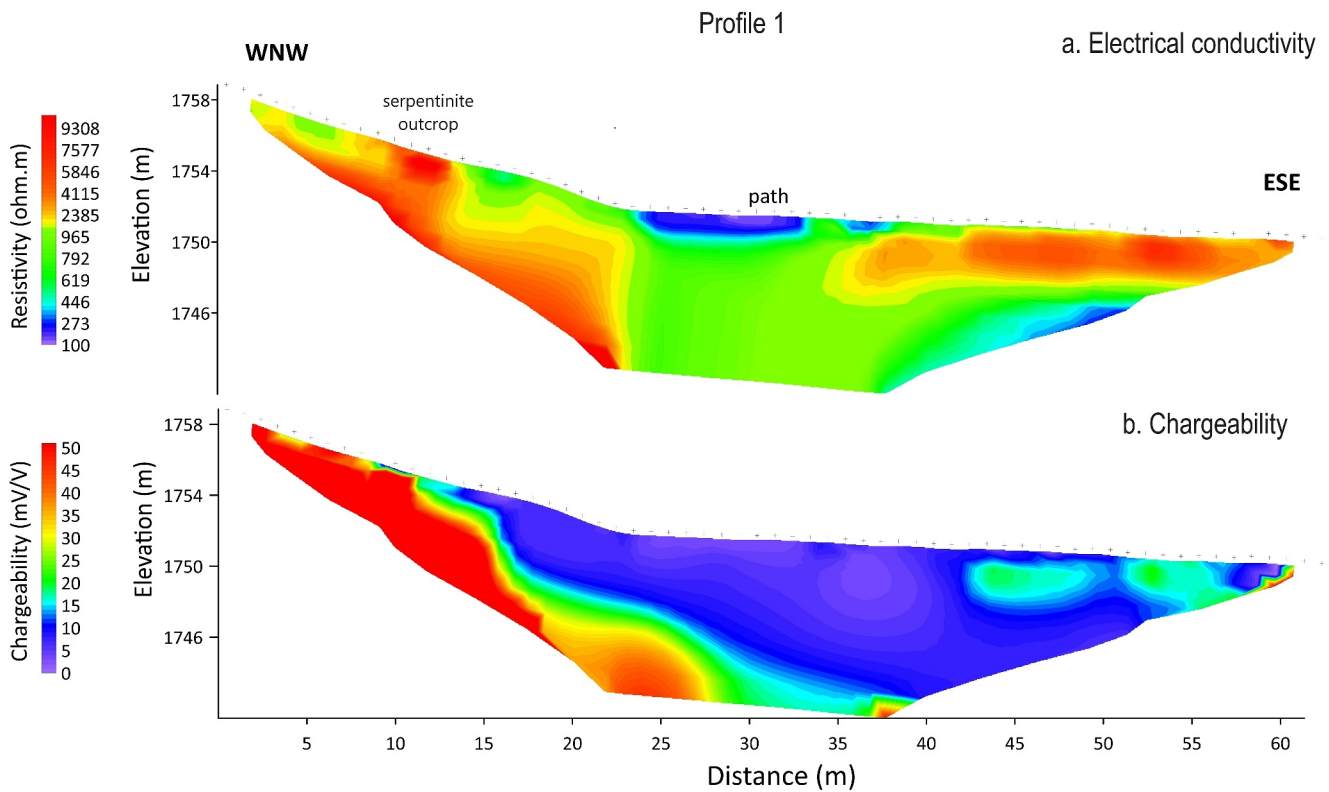


**Figure 2.** Time-domain induced polarization survey showing the electrical resistivity ( $\Omega$  m) and chargeability (mV/V) for Profile 1. Serpentinite outcrops on the left side of the profile are characterized by a high chargeability ( $>20$  mV/V and reaching several hundreds of mV/V) and high resistivity (2,000–10,000  $\Omega$  m). The dots along the profile denote the position of the electrodes (64 per profile). The high chargeability is likely associated with the presence of magnetite while the high resistivity is associated with the low porosity of the formation. (a) Electrical resistivity tomogram. (b) Chargeability tomogram.

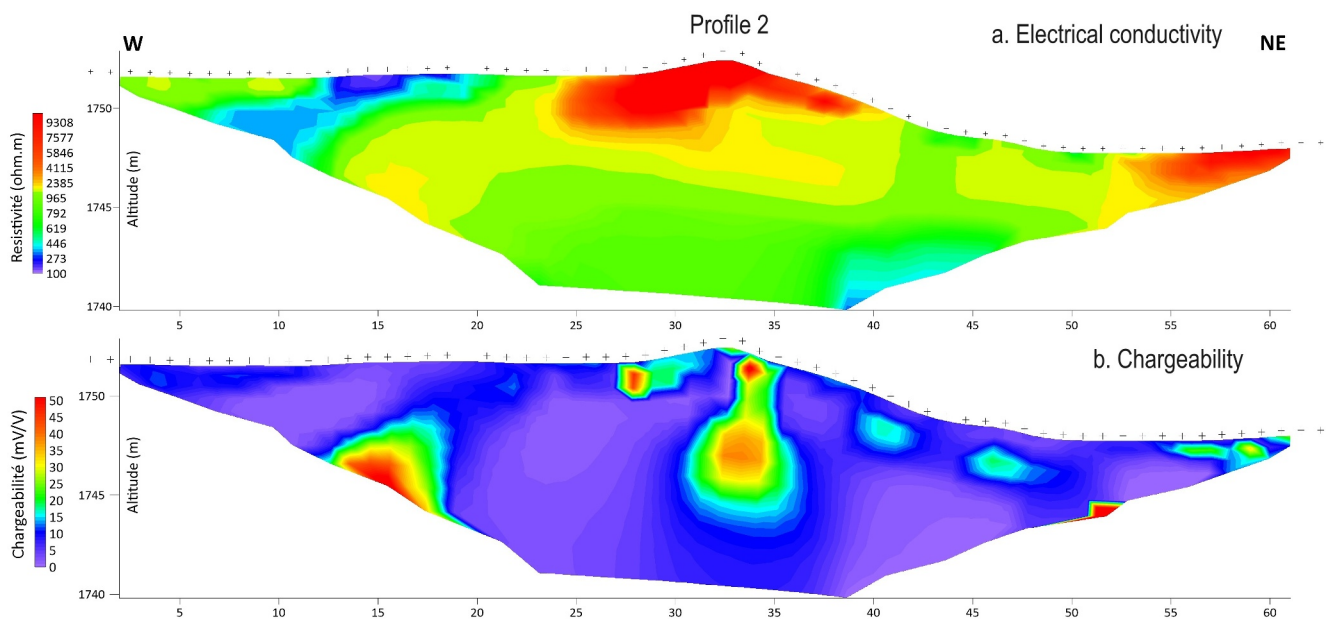


**Figure 3.** Time-domain induced polarization survey showing the electrical resistivity ( $\Omega$  m) and chargeability (mV/V) for Profile 2. We used the same scales as for Profile 1 in Figure 2. (a) Electrical resistivity tomogram. (b) Chargeability tomogram.



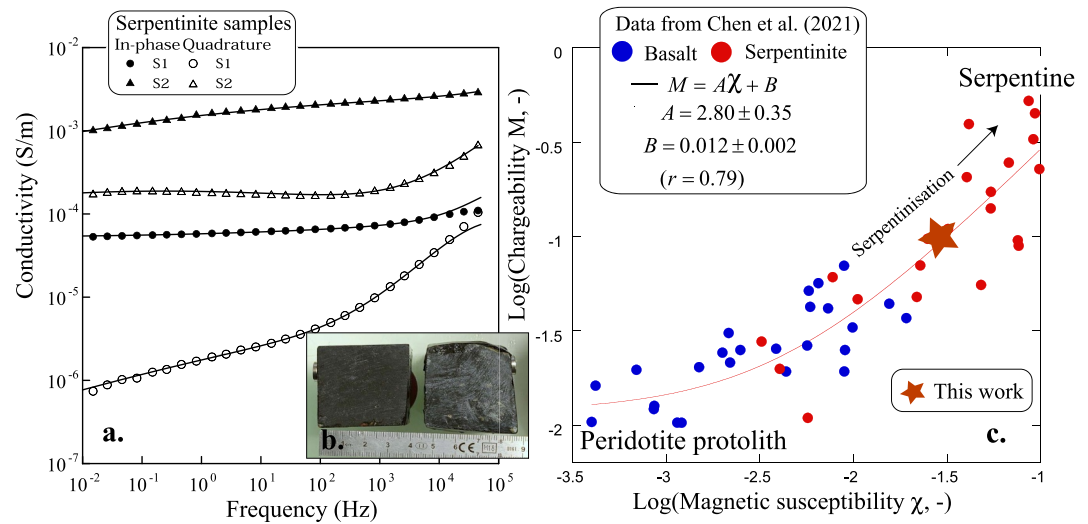


**Figure 4.** Petrophysical properties. (a) Complex conductivity spectrum (in phase and quadrature conductivity vs. frequency) for a core sample of serpentine from the outcrop of Profile 1. The plain line corresponds to a double Cole-Cole model. The low-frequency Cole-Cole model corresponds to the following values: the instantaneous conductivity is  $3.3 \times 10^{-4} \text{ S m}^{-1}$  ( $\sim 3,100 \text{ } \Omega \text{ m}$ ), the Cole-Cole exponent is 0.2, the relaxation time is  $8 \times 10^{-5} \text{ s}$  and the low frequency chargeability is 0.1 (100 mV/V). (b) A magnet sticks to the surface of the two core sample because of their high magnetite (possibly maghemite) content. (c) Chargeability  $M$  versus magnetic susceptibility  $\chi$  as an indicator of the serpentinization process.

steel electrodes were connected to the take-outs for each profile. The data were acquired both in resistivity and chargeability. The primary injection time was setup to 1 s while the secondary voltage was recorded for 1.2 s after the primary current was shut down. A dead time of 0.2 s was used after shutting down the primary current to avoid spurious electrode voltages associated with inductive and capacitive electromagnetic effects. The apparent chargeabilities were obtained by integrating the secondary voltage over windows of 100 ms. The first window is used to define the apparent chargeability, which is inverted to obtain a chargeability tomogram. We used the Wenner- $\alpha$  electrode array for its good signal-to-noise ratio, especially in the context of induced polarization measurements. The effect of electrode polarization was minimized by avoiding using any electrodes utilized for the current injection/retrieval for at least 10 min as voltage electrode. Every acquisition results in 472 measurements recorded per profile. The results were inverted with RES2DINV (Loke & Barker, 1996).

In order to analyze the facies associated with serpentine, we used one core sample from the outcrop located at the start of Profile 1 (Figure 1b). Great care should be done with such an approach since for instance fluid content and fracture density can change the resistivity by orders of magnitude. So while good for exposed and near surface rocks, rocks buried deeper could have very different petrophysical properties. The sample was cut in a cube with a side length of 4 cm. It was saturated under vacuum with tap water (conductivity at 25°C,  $0.1 \text{ S m}^{-1}$ ) during 4 weeks. Subsequently, we performed the spectral induced polarization measurements in the frequency range 10 mHz–45 kHz with the impedance meter developed by Zimmermann et al. (2008). The complex conductivity response is fitted with a Cole-Cole model and the results are shown in Figure 4a. We determined that the resistivity and the chargeability of the core sample are  $\sim 7,100 \text{ } \Omega \text{ m}$  and  $\sim 100 \text{ mV/V}$  for sample S1 and  $\sim 500 \text{ } \Omega \text{ m}$  and  $\sim 100 \text{ mV/V}$  for Sample S2. These data are consistent with the field induced polarization properties of the weathered serpentine found at the outcrop in Profile 1 (Figure 2) and suggest the potential presence of boulders of serpentine in Profile 2 (Figure 3).

Volumetric magnetic susceptibility at room temperature was measured using an AGICO Kappabridge with a magnetic field of  $200 \text{ A m}^{-1}$  (Chen et al., 2021). The measurement was averaged from five chip specimens ( $\sim 1 \text{ cm}^3$ ) extracted from the core samples. The sensitivity is  $2 \times 10^{-8} \text{ SI}$ . The serpentine core sample reached a high susceptibility value of  $0.0340 \pm 0.0005 \text{ SI}$ , which is comparable to the highly serpentinized peridotites with high magnetite abundance reported from mid-ocean ridges (see Figure 4b and Bonnemains et al., 2016; Chen et al., 2021).

#### 4. Clustering and Electrofacies

Our goal here is to use data clustering to define electrofacies in the data set using the electrical conductivity and chargeability distributions obtained after performing the least-square inversion. At first, we use 2D Resistivity and time domain induced polarization inversion to determine the subsurface resistivity and IP sections using a least-square technique and smoothness as regularization technique. In the second step, the logarithmic of the inverted resistivity and chargeability data are normalized. This is to build a distance metric. Finally, K-means clustering techniques are run to define electrofacies using values from each model cell. These electrofacies can correspond to geological units or alteration degrees of the same facies but are defined through their electrical properties.

The natural groups (clusters) are identified via similarity measures. These similarity measures include distance, connectivity, and intensity. Objects that belong to the same cluster are similar to one another and distinct from objects that belong to different clusters. The major types are hierarchal, distribution-based, density-based, and centroid-based clustering.

The K-means clustering algorithm proposed by MacQueen (1967) is a partition-based cluster analysis method. It is used widely in cluster analysis for that the K-means algorithm has higher efficiency and scalability and converges. K-means is used in many geophysical research in order to detect geophysical anomalies, outliers in geophysical data, hidden patterns, and interesting geological phenomena (e.g., Bedrosian et al., 2007; Di Giuseppe et al., 2014, 2018; Jing et al., 2021; Kuhn et al., 2019; Le et al., 2016; X. Wang et al., 2018; Xing et al., 2023).

The K-means clustering algorithm aims to partition  $n$  datapoint into  $k$  clusters in which each datapoint belongs to the cluster with the nearest mean.

The method starts with an initial guess for the cluster centers, which are intended to mark the mean location of each cluster. By iteratively updating the cluster centers, K-means clustering iteratively moves the cluster centers to the right location within a data set. This iteration is based on minimizing an objective function that represents the distance from any given data point to a cluster center:

$$\phi_{\text{K-means}} = \sum_{j=1}^k \sum_{x_i \in c_j} \|x_i - c_j\|^2, \quad (1)$$

where  $n$  denotes the number of datapoints to be clustered,  $c$  is the number of clusters to be discovered,  $x_i$  is the  $i$ th data object, and  $c_j$  is the center of the  $j$ th cluster.

Clustering models use a distance metric to measure similarities between observations and form clusters. So, features with high ranges will have a bigger influence on the clustering. Therefore, standardization is required before building a clustering model. For standardization, we used a standard normal distribution where the mean is 0 and the standard deviation is 1.

To improve the selection of initial centroids, we applied the Akaike Information Criterion and Bayesian Information Criterion methods to determine the optimal number of clusters. The best results were obtained using 4 and 5 clusters, respectively. The clustering shown in Figure 5 shows four distinct clusters. Additionally, we plotted a point representing the serpentinite samples (taken from the outcrop) in Figure 4a. The point shows at the margin of the cluster corresponding to the serpentinite. This may be the results of weathering with magnetite replaced by maghemite (another semi-conductor). The petrophysical data is consistent with the cluster corresponding to the facies outcropping at the beginning of Profile 1, as highlighted in Figure 2 and is therefore associated with serpentinite. Figure 6 shows the four electrofacies associated with the four clusters obtained with the K-means analysis. By correlating field observations of the exposed geological formations with the electrofacies, we can identify the continuity of the various sedimentary formations present at this site and the layout of the serpentinites at depth. We are also able to identify isolated blocks of serpentinites embedded in the sedimentary formations (Profile 2), indicating geological reworking and transport processes of the ophiolitic serpentinites possibly associated with detachment faulting (Figure 6b).

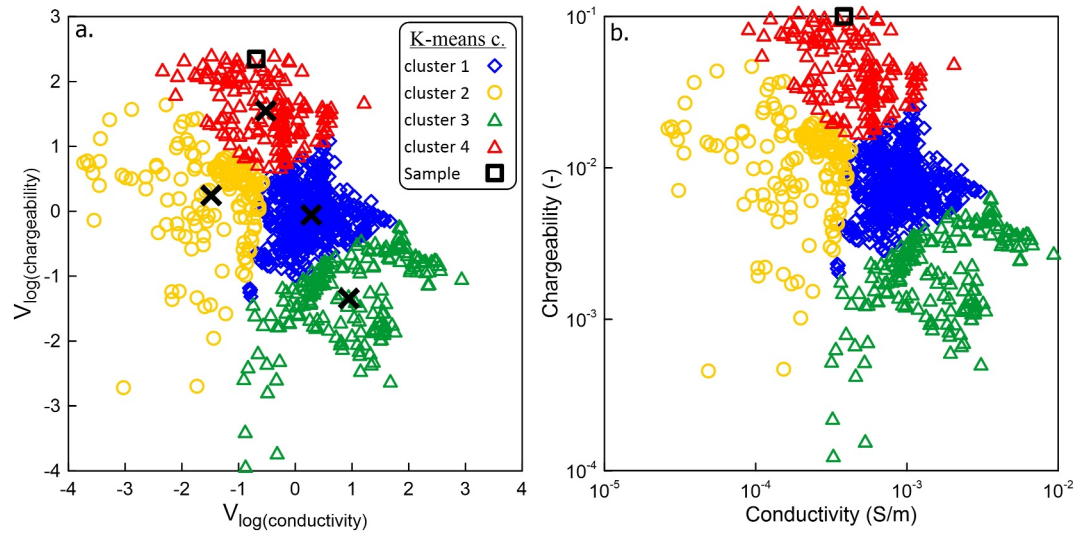


**Figure 5.** Clustering techniques applied to a cross plot between the chargeability data and the resistivity for the survey shown in Figures 2 and 3. The conductivity and chargeability data are normalized on the left-side plot in which the clustering technique is applied (unnormalized in the right-side plot). We can define four clusters with the crosses corresponding to the cluster barycenters in the normalized plot. (a) Cross-plot of the normalized parameters used to define the clusters for the field data. (b) Distribution of the clusters in a lot of the chargeability (in log scale) versus the electrical conductivity (in log scale).

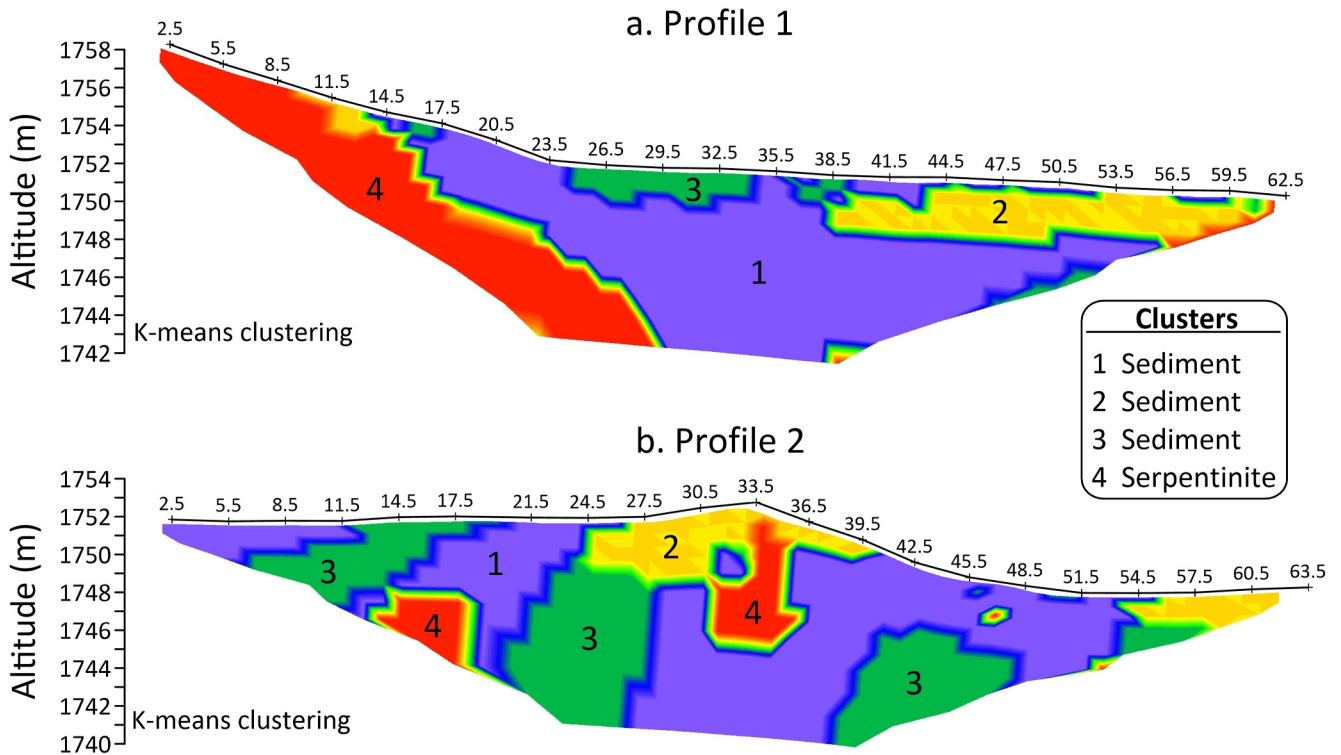


**Figure 6.** Results from the K-means clustering. Facies 1: alluvium with sandy loamy matrix, Facies 2: alluvium with coarse material rich in serpentinites blocks and located above the aquifer. Facies 3: Undefined sediments associated with a path. Facies 4: Serpentine and plurimetric serpentinite blocks. (a) Result for Profile 1. (b) Result for Profile 2.

## 5. Conclusions

We took advantage of the unique opportunity of an ophiolite outcrop in the Alps to image a serpentinite formation using time-domain induced polarization. One core sample of serpentinite and a clustering technique applied to the cross-plot between the chargeability and the electrical resistivity were used to identify four clusters, one of them being associated with the serpentinite and the three others with sedimentary formations. The results found in this paper can be used for exploring the evolution of serpentinization, that is, the hydration of geodynamic setting at the seafloor using the induced polarization technique. Note that caution should be used in using samples from an outcrop as water content and fracture density may change the petrophysical properties of interest. Furthermore, going from electrofacies to lithofacies and alteration degrees requires a ground truth to identify what each cluster represents. That said, this approach could be moved to the next step, which is petrophysically guided joint inversions, for instance of seismic and induced polarization data. Recently, we have started to use resistivity and self-potential to perform joint interpretation of sea floors mound like TAG (Su et al., 2022). The next step will be to add large scale induced polarization measurements in Controlled Source ElectroMagnetic measurements. In that respect, the magnetite fraction (~5%) in natural serpentinites is too low to produce a conductive network able to influence the conductivity of these materials. Hence, the properties of the aqueous fluid phase (water content and salinity) are of importance to the conductivity structure of serpentinized systems. A fluid salinity of 10 wt.% (several times higher than seawater) cause a higher conductivity than in the present work for which the pore water is composed of fresh pore water of meteoritic origin. The serpentinite in the lower crust can be more conductive as shown above. This conductive structure is very sensitive to the fluid content and salinity and not to serpentinization (Falcon-Suarez et al., 2017; Q. Wang & Bagdassarov, 2013). This is why the induced polarization used in our paper is expected to provide more insights into serpentinized structures.

## Data Availability Statement

The data used in the present paper can be found at the repository ZENODO <https://zenodo.org> with the doi reference <https://doi.org/10.5281/zenodo.10684241>. The first two files (Data 1 and Data 2) comprise the geophysical survey as a .DAT file with the apparent resistivity and chargeability data. The format can be read by RES2DINV (available in the Aarhus GeoSoftware website via <https://www.aarhusgeosoft.dk/download-resx2dinv>, under commercial licensing, and is accessible to the public or research community as a demo/display version). RES2DINV Version 6.2 was used for inversion of the apparent resistivity and chargeability data sets.

## Acknowledgments

This work is supported by the CNRS and the Université Savoie Mont-Blanc (USMB). A. Revil thanks E. Zimmermann for the IP equipment used for the laboratory experiment and we thank Gabriel Parcillié for his work on the field data.

## References

- Bedrosian, P. A., Maercklin, N., Weckmann, U., Bartov, Y., Ryberg, T., & Ritter, O. (2007). Lithology-derived structure classification from the joint interpretation of magnetotelluric and seismic models. *Geophysical Journal International*, 170(2), 737–748. <https://doi.org/10.1111/j.1365-246X.2007.03440.x>
- Bonnemains, D., Carlut, J., Escartín, J., Mével, C., Andreani, M., & Debret, B. (2016). Magnetic signatures of serpentinization at ophiolite complexes: Magnetism of ophiolite serpentinites. *Geochemistry, Geophysics, Geosystems*, 17(8), 2969–2986. <https://doi.org/10.1002/2016GC006321>
- Carlson, R. L., & Miller, D. J. (1997). A new assessment of the abundance of serpentinite in the oceanic crust. *Geophysical Research Letters*, 24(4), 457–460. <https://doi.org/10.1029/97GL00144>
- Chen, H., Tao, C., Revil, A., Zhu, Z., Zhou, J., Wu, T., & Deng, X. (2021). Induced polarization and magnetic responses of serpentinized ultramafic rocks from mid-ocean ridges. *Journal of Geophysical Research: Solid Earth*, 126(12), e2021JB022915. <https://doi.org/10.1029/2021JB022915>
- Chopin, C. (1979). *De la Vanoise au massif du Grand Paradis. Une approche pétrographique et radiochronologique de la signification géodynamique du métamorphisme de Haute pression*. PhD thesis (p. 145). University Pierre et Marie Curie Paris.
- Colletini, C., Viti, C., Smith, S. A. F., & Holdsworth, R. E. (2009). Development of interconnected talc networks and weakening of continental low-angle normal faults. *Geology*, 37(6), 567–570. <https://doi.org/10.1130/G25645A.1>
- Decrausaz, T., Müntener, O., Manzotti, P., Lafay, R., & Spandler, C. (2021). Fossil oceanic core complexes in the Alps. New field, geochemical and isotopic constraints from the Tethyan Aiguilles Rouges ophiolite (Val d'Hérens, Western Alps, Switzerland). *Swiss Journal of Geosciences*, 114(3), 3. <https://doi.org/10.1186/s00015-020-00380-4>
- Deville, E. (1987). *Etude géologique en Vanoise orientale (Alpes occidentales françaises, Savoie). De la naissance à la structuration d'un secteur de la paléomarge européenne et de l'océan Téthysien: Aspects stratigraphiques, pétrographiques et tectoniques* (p. 298). Thèse Université de Savoie.
- Di Giuseppe, M. G., Troiano, A., Patella, D., Piochi, M., & Carlino, S. (2018). A geophysical k-means cluster analysis of the Solfatara-Pisciarelli volcano-geothermal system, Campi Flegrei (Naples, Italy). *Journal of Applied Geophysics*, 156, 44–54. <https://doi.org/10.1016/j.jappgeo.2017.06.001>
- Di Giuseppe, M. G., Troiano, A., Troise, C., & De Natale, G. (2014). K-means clustering as tool for multivariate geophysical data analysis. An application to shallow fault zone imaging. *Journal of Applied Geophysics*, 101, 108–115. <https://doi.org/10.1016/j.jappgeo.2013.12.004>
- Dilek, Y. (2003). Ophiolite concept and its evolution. In Y. Dilek & S. Newcomb (Eds.), *Ophiolite concept and the evolution of geological thought* (Vol. 373, pp. 1–16). Geological Society of America Special Paper. <https://doi.org/10.1130/0-8137-2373-6.1>



- Falcon-Suarez, I., Bayrakci, G., Minshull, T. A., North, L. J., Best, A. I., & Rouméjon, S. (2017). Elastic and electrical properties and permeability of serpentinites from Atlantis Massif, mid-Atlantic ridge. *Geophysical Journal International*, 211(2), 686–699. <https://doi.org/10.1093/gji/ggx341>
- Fudral, S. (1998). Etude géologique de la suture téthysienne dans les Alpes franco-italiennes nord-occidentales de la Doire Ripaire (Italie) à la région de Bourg-Saint-Maurice (France). *Géologie Alpine*, Mémoire HS 29 (p. 306).
- Hacker, B. R. (1990). Simulation of the metamorphic and deformational history of the metamorphic sole of the Oman ophiolite. *Journal of Geophysical Research*, 95(B4), 4895–4907. <https://doi.org/10.1029/JB095iB04p04895>
- Jing, J., Ke, S., Li, T., & Wang, T. (2021). Energy method of geophysical logging lithology based on K-means dynamic clustering analysis. *Environmental Technology & Innovation*, 23, 101534. <https://doi.org/10.1016/j.eti.2021.101534>
- Kuhn, S., Cracknell, M. J., & Reading, A. M. (2019). Lithological mapping in the Central African copper belt using random forests and clustering: Strategies for optimised results. *Ore Geology Reviews*, 112, 103015. <https://doi.org/10.1016/j.oregeorev.2019.103015>
- Lagabrielle, Y. (1994). Ophiolites of the southwestern Alps and the structure of the Tethyan oceanic lithosphere. *Ophioliti*, 19, 413–434.
- Le, C. V. A., Harris, B. D., Pethick, A. M., Takougang, E. M. T., & Howe, B. (2016). Semiautomatic and automatic cooperative inversion of seismic and magnetotelluric data. *Surveys in Geophysics*, 37(5), 845–896. <https://doi.org/10.1007/s10712-016-9377-z>
- Loke, M. H., & Barker, R. D. (1996). Rapid least-squares inversion of apparent resistivity pseudosections by a quasi-Newton method. *Geophysical Prospecting*, 44(1), 131–152. <https://doi.org/10.1111/j.1365-2478.1996.tb00142.x>
- MacQueen, J. (1967). Some methods for classification and analysis of multivariate observations. In *Proceedings of the fifth Berkeley symposium on mathematical statistics and probabilities* (Vol. 1, pp. 281–296).
- Nicoud, G., Bourlès, D., Hyppolite, J.-C., Coutterand, S., & Paillet, A. (2009). *Sur l'âge Dryas récent des moraines frontales du Villaron à Bessans. Implications dans la lithostratigraphie locale de la déglaciation de la haute vallée de l'Arc (Maurienne, Savoie-France). Rencontres datation. Les formations superficielles en domaine continental: apport des nouvelles méthodes de datation. Le point sur les méthodes de datation. Application aux stratigraphies locale et régionale. June 4th, 2009.* Université Paul Valéry, Montpellier III.
- Raguin, E. (1929). Subdivision de la nappe des schistes lustrés en Haute-Maurienne. *C.R. Acad. Sci., Paris*, 189, 934–936. Retrieved from <https://pascal-francis.inist.fr/vibad/index.php?action=getRecordDetail&idt=GEODEBRGMFR1326613>
- Revil, A. (2013). On charge accumulations in heterogeneous porous materials under the influence of an electrical field. *Geophysics*, 78(4), D271–D291. <https://doi.org/10.1190/GEO2012-0503.1>
- Robert, D. (1979). *Contribution à l'étude géologique de la Haute-Vallée de l'Arc. Région de Bonneval (Savoie)*. Ph.D. Thesis (p. 181). Pierre and Marie Curie University.
- Schlumberger, C. (1920). *Etude sur la prospection électrique du sous-sol*. Gauthier-Villars. Retrieved from <https://archive.org/details/studyofundergrou00schlrich/page/n37>
- Su, Z., Tao, C., Zhu, Z., Revil, A., Shen, J., Nie, Z., et al. (2022). Joint interpretation of marine self-potential and transient electromagnetic survey for seafloor massive sulfide (SMS) deposits: Application at TAG hydrothermal mound, Mid-Atlantic Ridge. *Journal of Geophysical Research: Solid Earth*, 127(11), e2022JB024496. <https://doi.org/10.1029/2022JB024496>
- Toft, P. B., Arkani-Hamed, J., & Haggerty, S. E. (1990). The effects of serpentinization on density and magnetic susceptibility: A petrophysical model. *Physics of the Earth and Planetary Interiors*, 65(1–2), 137–157. [https://doi.org/10.1016/0031-9201\(90\)90082-9](https://doi.org/10.1016/0031-9201(90)90082-9)
- Vinciguerra, S., & Bernabé, Y. (2009). *Rock physics and natural hazards, Pageoph topical volume* (p. 739). Springer, Birkhauser.
- Wang, Q., & Bagdassarov, N. (2013). The Moho as a transition zone: A revisit from seismic and electrical properties of minerals and rocks. *Tectonophysics*, 609, 395–422. <https://doi.org/10.1016/j.tecto.2013.08.041>
- Wang, X., Yang, S., Zhao, Y., & Wang, Y. (2018). Lithology identification using an optimized KNN clustering method based on entropy-weighted cosine distance in Mesozoic strata of Gaoqing field, Jiyang depression. *Journal of Petroleum Science and Engineering*, 166, 157–174. <https://doi.org/10.1016/j.petrol.2018.03.034>
- Xing, Y., Yang, H., & Yu, W. (2023). An approach for the classification of rock types using machine learning of core and log data. *Sustainability*, 15(11), 8868. <https://doi.org/10.3390/su15118868>
- Zimmermann, E., Kemna, A., Berwix, J., Glaas, W., Münch, H. M., & Huisman, J. A. (2008). A high-accuracy impedance spectrometer for measuring sediments with low polarizability. *Measurement Science and Technology*, 19(10), 105603. <https://doi.org/10.1088/0957-0233/19/10/105603>